DOI: https://doi.org/10.15625/0868-3166/21623

# Joint polarizations of W pair production at the LHC at NLO QCD+EW accuracy

Thi Nhung Dao and Duc Ninh Le<sup>†</sup>

Phenikaa Institute for Advanced Study, Phenikaa University, Hanoi 12116, Vietnam

*E-mail*: †ninh.leduc@phenikaa-uni.edu.vn

Received 30 September 2024; Accepted for publication 4 April 2025; Published 10 June 2025

**Abstract.** In this contribution, we present new results of next-to-leading order (NLO) electroweak corrections to the doubly polarized  $W^+W^-$  production cross sections at the LHC, via the full leptonic final state. This calculation has been recently achieved independently by two groups: one in Germany and our group in Vietnam. A comparison of the two results will be presented. We include also the NLO QCD corrections in the numerical analysis since they are dominant and therefore important for comparison with experimental results. New results of integrated cross section for future proton-proton colliders with  $\sqrt{s} = 27 \, \text{TeV}$ , 50 TeV, 100 TeV are provided. Moreover, a detailed explanation of the  $\sigma_{TT} > \sigma_{LT} > \sigma_{LL}$  hierarchy based on the Born approximation is given.

Keywords: LHC; diboson production; polarization; NLO; electroweak; QCD.

Classification numbers: 12.15.-y; 14.70.Fm; 14.70.Hp.

#### 1. Introduction

Polarization of a massive gauge boson has attracted attention since the discovery of the Standard Model (SM) and the subsequent observation of the  $W^{\pm}$  and Z bosons at the CERN proton-antiproton collider SPS (Super Proton Synchrotron) in 1983.

Since then, a lot of theoretical and experimental works have been performed. Notably, the polarization fractions for  $e^+e^- \to W^+W^-$  process have been measured at LEP by the OPAL [1] and DELPHI [2] collaborations. More recently, at the LHC, joint-polarized cross sections in  $W^\pm Z$ , ZZ, and same-sign  $W^\pm W^\pm jj$  productions have been reported in [3, 4] (ATLAS), [5] (ATLAS), and [6] (CMS), respectively.

On the theoretical side, the recent next-to-leading order (NLO) QCD and electroweak (EW) predictions for doubly-polarized cross sections have been provided for ZZ [7],  $W^{\pm}Z$  [8–10],  $W^{+}W^{-}$  [11–14], for fully leptonic decays. Next-to-next-to-leading order (NNLO) QCD results have been obtained for  $W^{+}W^{-}$  [15]. Semileptonic final state has been considered in [16] for the

This is an extended version of the talk presented at the 49th Vietnam Conference on Theoretical Physics, Hue, Vietnam (2024).

case of WZ at NLO QCD, in [17] for triboson production at NLO QCD+EW, and in [18] for vector boson scattering at leading order (LO).

Going beyond the fixed order, new results in [19] show that it is now possible to simulate polarized events, for multi-boson production processes, at the precision level of approximate fixed-order NLO QCD corrections matched with parton shower using the Monte-Carlo generator SHERPA. In addition, the above full NLO QCD calculations in ZZ [7],  $W^{\pm}Z$  [8],  $W^{+}W^{-}$  [11] have been implemented in the POWHEG-BOX framework [20], thereby incorporating parton-shower effects. Very recently, polarized ZZ pairs via gluon fusion have been generated using the combination of FeynRules and MadGraph5\_aMC@NLO [21], allowing for another option of realistic simulation.

In this contribution, we report on the new finding of Ref. [13] for the  $pp \to W^+W^- \to e^+ v_e \mu^- \bar{v}_\mu$  process at NLO QCD+EW and perform a comparison to the NLO EW results of Ref. [12] which was published on arXiv one day before ours. The content of this report is significantly improved in comparison to the talk presented at the conference in the following respects: (i) the references are updated to include a few new relevant articles which have been published since the talk, (ii) a few comments are added to make connection to our new publication [14], (iii) a detailed explanation of the  $\sigma_{TT} > \sigma_{LT} > \sigma_{LL}$  hierarchy based on the Born approximation is provided, (iv) integrated cross sections for future proton-proton colliders with  $\sqrt{s} = 27 \, \text{TeV}$ , 50 TeV, 100 TeV are given. Other numerical results for the case of 13 TeV are the same as those presented at the talk.

#### 2. Calculation method

In order to separate the different polarization contributions of the  $W^+W^-$  system, we use the Double Pole Approximation (DPA) [22–24] which works in three steps:

- Select all diagrams with 2 s-channel resonances:  $W^+ \to e^+ \nu_e$ ,  $W^- \to \mu^- \bar{\nu}_\mu$ ;
- Factorize the amplitude into production and decay parts, and replace the propagators of the resonances by the Breit-Wigner formulae;
- Apply an on-shell projection on the momenta of the production process and on the momenta of the decays to make each production and decay amplitudes gauge invariant.

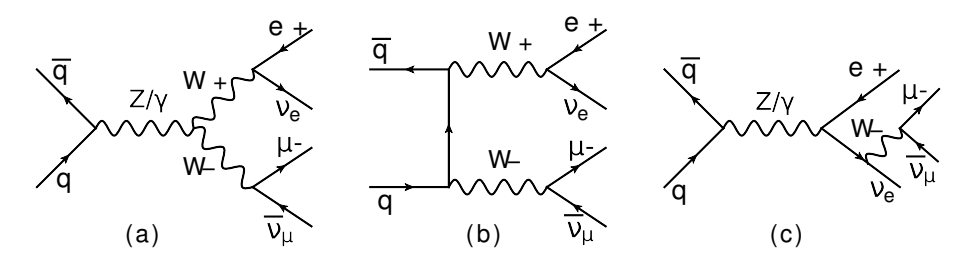


**Fig. 1.** Representative Feynman diagrams at leading order. Diagrams (a) and (b) are doubly resonant hence included in the DPA, while (c) is excluded.

The first step can be better understood by looking at the leading order diagrams in Fig. 1. The doubly resonant diagrams (a) and (b) are selected for the DPA while the singly resonant diagram (c) is excluded.

In the second step, the unpolarized amplitude is then factorized at leading order as follows (writing  $V_1 = W^+$ ,  $V_2 = W^-$ ,  $l_1 = e^+$ ,  $l_2 = v_e$ ,  $l_3 = \mu^-$ ,  $l_4 = \bar{v}_{\mu}$ ):

$$\mathscr{A}_{\text{LO,DPA}}^{\bar{q}q \to V_1 V_2 \to 4l} = \frac{1}{Q_1 Q_2} \sum_{\lambda_1, \lambda_2 = 1}^{3} \mathscr{A}_{\text{LO}}^{\bar{q}q \to V_1 V_2}(\hat{k}_i, \lambda_1, \lambda_2) \mathscr{A}_{\text{LO}}^{V_1 \to l_1 l_2}(\hat{k}_i, \lambda_1) \mathscr{A}_{\text{LO}}^{V_2 \to l_3 l_4}(\hat{k}_i, \lambda_2), \tag{1}$$

with

$$Q_{j} = q_{j}^{2} - M_{V_{j}}^{2} + iM_{V_{j}}\Gamma_{V_{j}} \quad (j = 1, 2),$$
(2)

where  $q_1 = k_3 + k_4$ ,  $q_2 = k_5 + k_6$ ,  $M_{V_j}$  and  $\Gamma_{V_j}$  are the physical mass and width of the gauge boson  $V_j$ , and  $\lambda_j$  are the polarization indices of the gauge bosons. Notice that, different from the narrow width approximation, the off-shell momenta are kept in the denominator of the gauge boson propagators to better describe the two resonances.

For Eq. (1) to be gauge invariant, we have to make each amplitude factor in the r.h.s. gauge invariant. This is achieved by requiring that the momentum set of each amplitude is on-shell, meaning they satisfy the condition  $\hat{k}_i^2 = m_i^2$  with  $m_i$  being the physical mass of the *i*-th particle of the production or decay process. To distinguish the on-shell momenta, we denote them with a hat.

In practice, the on-shell momenta  $\hat{k}_i$  are calculated from the off-shell momenta  $k_i$  using an on-shell mapping. This mapping is not unique and different mappings give different results. The differences are very small, of order  $\alpha\Gamma_V/(\pi M_V)$  [24], being the intrinsic uncertainty of the DPA due to a finite width. In the present work, we use the LO on-shell mapping DPA<sup>(2,2)</sup> as defined in [7]. This completes the description of the third step mentioned above.

The above procedure can be extended for NLO QCD and EW corrections. The Catani-Seymour subtraction method [25] is very useful and applied here. The massive dipoles are provided in [26] for dimensional regularization and in [27] for mass regularization for production processes. The dipole subtraction method for decay processes was developed in [28]. We need the massive dipoles because both the production and decay processes have massive gauge bosons in the external legs. Note that, even though the massive dipole terms provided in [26–28] are for fermions, they can be used for gauge bosons as well, because the soft singularity structure is identical for fermions and bosons (see e.g. Eq. (7.13) of [29]) and the collinear singularity (which is spin dependent) does not cause problems for the W bosons due to their large mass compared to the collision energy at the LHC.

The implementation of the Catani-Seymour method in the DPA is nontrivial because we have to deal with two kinds of mappings, the on-shell mappings (on-shell limits) and the Catani-Seymour mappings (soft and collinear limits), which do not commute. The order to apply them was specified in [10, 13], see also [7, 12]. In this work, we follow the method of [10, 13], where the reader can find all the calculation details.

It is important to note that the separation of the unpolarized amplitude into a sum of polarized amplitudes as in Eq. (1) must be done for all NLO EW correction processes: virtual, photon radiation, quark-photon induced processes (and similarly for NLO QCD corrections). In this way, we can define polarized cross sections at NLO by summing up all the corrections for a given polarization (e.g. selecting  $\lambda_1 = \lambda_2 = 2$  for the LL polarization).

Since each massive gauge boson has three polarization states, two transverse modes ( $\lambda = 1,3$  in Eq. (1)) and one longitudinal mode ( $\lambda = 2$  in Eq. (1)); the unpolarized cross section, being proportional to the unpolarized amplitude squared, can be separated into five terms:

$$\sigma_{\text{unpol}} = \sigma_{\text{LL}} + \sigma_{\text{LT}} + \sigma_{\text{TL}} + \sigma_{\text{TT}} + \sigma_{\text{interf}}, \tag{3}$$

where  $\sigma_{LL} \propto |\mathcal{A}_{22}|^2$ ,  $\sigma_{LT} \propto |\mathcal{A}_{21} + \mathcal{A}_{23}|^2$  (a coherent sum of the  $\mathcal{A}_{21}$  and  $\mathcal{A}_{23}$  amplitudes),  $\sigma_{TL} \propto |\mathcal{A}_{12} + \mathcal{A}_{32}|^2$ ,  $\sigma_{TT} \propto |\mathcal{A}_{11} + \mathcal{A}_{13} + \mathcal{A}_{31} + \mathcal{A}_{33}|^2$ . The last term is the interference between the LL, LT, TL, and TT amplitudes. This interference term vanishes if the integration over the full phase space of the decay products is performed [11]. This is however not the case in realistic calculations as kinematic cuts are applied to the decay products, leading to a non-vanishing interference.

We note that while the unpolarized cross section is Lorentz invariant the individual polarized cross sections in the r.h.s. are not Lorentz invariant. Their values therefore are reference frame dependent. Various choices can be made, including the Laboratory frame, the partonic frame, or the VV center-of-mass frame. In this work, we will choose the VV frame, as it is the most natural choice to study the polarization of a diboson system.

We now come to our computer tools. The numerical results of this work are obtained using our in-house computer program MulBos (MultiBoson production), which has been used for our previous papers [9, 10, 13, 14]. The ingredients of this program include the helicity amplitudes for the production and decay processes, generated by FeynArt [30] and FormCalc [31], an inhouse library for one-loop integrals named LoopInts. The tensor one-loop integrals are calculated using the standard technique of Passarino-Veltman reduction [32], while the scalar integrals are computed as in [33–35]. The phase space integration is done using the Monte-Carlo integrator BASES [36], with the help of useful resonance mapping routines publicly available in VBFNL0 [37]. Our code has been carefully checked by making sure that all UV and IR divergences cancel and singular limits of the dipole subtraction terms behave correctly. Comparisons with the results of [7,8,11,12] have been done for all ZZ, WZ and  $W^+W^-$  processes, showing good agreements. The largest discrepancy is at the level of 0.4% for the  $W^+W^-$  case, which will be discussed more later.

### 3. Numerical results

Using the ATLAS setup of (with  $\ell = e, \mu$ , missing energy is due to the neutrinos)

$$p_{T,\ell} > 27 \,\text{GeV}, \quad p_{T,\text{miss}} > 20 \,\text{GeV}, \quad |\eta_{\ell}| < 2.5, \quad m_{e\mu} > 55 \,\text{GeV},$$
  
jet veto (no jets with  $p_{T,j} > 35 \,\text{GeV}$  and  $|\eta_{j}| < 4.5$ ), (4)

where the jet veto is used to suppress the top-quark and other QCD backgrounds, we obtain the following results for the integrated polarized cross sections, see Table 1.

For the second to fourth columns, the cross sections include only the light quark induced processes (u, d, c, s). We will denote the light quark induced processes as  $q\bar{q}$ , which consists of also the quark-gluon and quark-photon induced processes at NLO. We see that the NLO QCD corrections are moderate because of the jet veto which reduces significantly the gluon-quark induced contribution. The EW corrections, denoted as  $\bar{\delta}_{\rm EW} = \Delta \sigma_{\rm EW}/\sigma_{\rm NLOQCD}$ , range from -2% to -5% for different polarizations. In addition, the sub-leading contributions from the loop-induced gluon-gluon fusion (gg), photon-photon fusion  $(\gamma\gamma)$ , and bottom-antibottom annihilation  $(b\bar{b})$  are also included in the  $\sigma_{\rm all}$ , and separately shown (relative to the NLOQCD results). These small

**Table 1.** Unpolarized and doubly polarized cross sections in fb calculated in the VV frame for the process  $pp \to W^+W^- \to e^+\nu_e\mu^-\bar{\nu}_\mu + X$ . The statistical uncertainties (in parenthesis) are given on the last digits of the central prediction when significant. Sevenpoint scale uncertainty is also provided for the cross sections as sub- and superscripts in percent. In the last column the polarization fractions are provided. Taken from [13].

	σ <sub>LO</sub> [fb]	$\sigma_{ m NLO}^{ m QCD}[{ m fb}]$	$\sigma_{ m NLO}^{ m QCDEW}$ [fb]	σ <sub>all</sub> [fb]	$\overline{\delta}_{\rm EW}$ [%]	$\overline{\delta}_{gg}[\%]$	$\overline{\delta}_{b\overline{b}}[\%]$	$\overline{\delta}_{\gamma\gamma}[\%]$	f <sub>all</sub> [%]
Unpolarized	$198.14(1)_{-6.5\%}^{+5.3\%}$	$210.91(3)^{+1.6\%}_{-2.2\%}$	202.90(3) <sup>+1.3%</sup> <sub>-1.9%</sub>	$222.41(3)^{+2.2\%}_{-2.5\%}$	-3.80	6.20	1.87	1.18	100
$W_L^+W_L^-$	12.99 <sup>+6.1%</sup> <sub>-7.4%</sub>	$14.03^{+1.9\%}_{-2.6\%}$	$13.64^{+1.7\%}_{-2.4\%}$	16.46 <sup>+4.7%</sup> <sub>-5.7%</sub>	-2.75	4.08	15.11	0.94	7.4
$W_L^+W_T^-$	21.67 <sup>+6.3%</sup> <sub>-7.5%</sub>	$24.86^{+1.8\%}_{-2.6\%}$	$24.28^{+1.7\%}_{-2.5\%}$	25.75 <sup>+2.6%</sup> <sub>-3.5%</sub>	-2.32	1.56	3.86	0.50	11.6
$W_T^+W_L^-$	$22.14_{-7.5\%}^{+6.2\%}$	25.56 <sup>+1.8%</sup> <sub>-2.6%</sub>	$24.96^{+1.7\%}_{-2.5\%}$	26.43 <sup>+2.6%</sup> <sub>-3.5%</sub>	-2.34	1.52	3.75	0.48	11.9
$W_T^+W_T^-$	$140.44^{+4.8\%}_{-6.0\%}$	$144.97(2)_{-1.9\%}^{+1.6\%}$	$138.42(2)_{-1.6\%}^{+1.4\%}$	152.95(3)+2.3%	-4.52	8.32	0.25	1.46	68.8
Interference	0.90(1)	1.50(4)	1.60(4)	0.81(4)					0.4

corrections are calculated at LO. The most interesting correction is from the  $b\bar{b}$  process, where a significant effect of +15% is found for the LL polarization. This large effect is due to the top-quark mass in the *t*-channel propagator. We have further investigated this effect at NLO QCD+EW level and presented our results in [14]. Finally, the polarization fractions ( $f_X = \sigma_X/\sigma_{\rm unpol}$ ) are provided in the last column, showing that the LL fraction is about 7%, the TT 69%, and the LT and TL 12% each. The interference is negligible, being 0.4%.

Explaining the hierarchy of the LL, LT, TL, LL cross sections takes a few steps. A good way to understand this hierarchy is using the LO results for the on-shell  $W^+W^-$  production process. The polarized amplitudes for the  $q(s_1,q_1) + \bar{q}(s_2,q_2) \rightarrow W^+(\lambda_1,p_1) + W^-(\lambda_2,p_2)$  process read

$$\mathscr{A}(s_1, s_2, \lambda_1, \lambda_2) = \epsilon^{\mu}(\lambda_1, p_1) \epsilon^{\nu}(\lambda_2, p_2) \mathscr{M}_{\mu\nu}(s_1, s_2, q_1, q_2), \tag{5}$$

where  $s_i$ ,  $q_i$  with i = 1, 2 are the helicity indices and momenta of the initial-state quarks,  $\lambda_i$ ,  $p_i$  the helicity indices and momenta of the W bosons. In the  $q\bar{q}$  center of mass system, the momenta read

$$q_1^{\mu} = (E, 0, 0, -E), \quad q_2^{\mu} = (E, 0, 0, +E);$$
  
$$p_1^{\mu} = (E, -p\sin\theta, 0, -p\cos\theta), \quad p_2^{\mu} = (E, +p\sin\theta, 0, +p\cos\theta),$$
 (6)

with  $E = (p^2 + M_W^2)^{1/2}$ ,  $p = |\mathbf{p}_1| = |\mathbf{p}_2|$ . The polarization vectors of the  $W^-$  are

$$\epsilon^{\mu}(+, p_2) = \frac{1}{\sqrt{2}}(0, \cos\theta, +i, -\sin\theta), \quad \epsilon^{\mu}(-, p_2) = \frac{1}{\sqrt{2}}(0, \cos\theta, -i, -\sin\theta);$$

$$\epsilon^{\mu}(L, p_2) = \frac{1}{M_W}(p, E\sin\theta, 0, E\cos\theta), \tag{7}$$

which satisfy the orthogonal condition of  $\epsilon(\lambda_2,p_2)\cdot p_2=0$  and the normalization of  $\epsilon^*(\lambda_2,p_2)\cdot \epsilon(\lambda_2',p_2)=-\delta_{\lambda_2,\lambda_2'}$ . The polarization vectors of the  $W^+$  are obtained by replacing  $\theta$  with  $(\theta+\pi)$ .

To extract the high energy limit of  $E \to \infty$ , we write the longitudinal polarization vector in the following form [38]

$$\epsilon^{\mu}(L, p_2) = ap_2^{\mu} + bp_1^{\mu}.$$
(8)

Upon contracting both sides with  $p_{2\mu}$  and  $p_{1\mu}$ ; and working in the WW center of mass system where  $p = \sqrt{s\beta/2}$  with  $s = (p_1 + p_2)^2 = 4E^2$ ,  $\beta = (1 - 4M_W^2/s)^{1/2}$ ; we can easily solve for a and b:

$$a = \frac{1+\beta^2}{2\beta M_W}, \quad b = -\frac{2M_W}{\beta s}.$$
 (9)

In the limit of  $E \to \infty$ , we have  $a \to 1/M_W$  and  $b \to 1/E^2$ , leading to

$$\epsilon^{\mu}(L, p_2) \to \frac{p_2^{\mu}}{M_W}.$$
(10)

We can see here an important difference between the logitudinal polarization and the transverse ones. While the transverse polarization vectors are independent of the energy, the  $\epsilon_L$  is proportional to E in the high energy limit.

With these ingredients, summing over s and t channel diagrams and neglecting the quark masses (the  $b\bar{b}$  process is here excluded), one obtains for the partonic cross sections [38]

$$\frac{d\hat{\sigma}_{LL}}{dt} = \frac{\pi\alpha^2}{48s_W^4\beta^4} \frac{ut - M_W^4}{s^2} \left[ \frac{1}{(s - M_Z^2)^2} (b_L^2 + b_R^2) + 2\rho^2 \frac{1}{s - M_Z^2} \frac{1}{t} b_L + \rho^4 \frac{1}{t^2} \right],\tag{11}$$

$$\frac{d\hat{\sigma}_{\text{TL+LT}}}{dt} = \frac{\pi\alpha^2}{48s_W^4\beta^4} \frac{\rho^2}{s^2} \left[ \frac{1}{(s-M_Z^2)^2} [s^2\beta^2 - 2(ut - M_W^4)](d_L^2 + d_R^2) \right]$$
(12)

$$-4\frac{1}{s-M_Z^2}\frac{1}{t}[s\beta^2(t-M_W^2)+(ut-M_W^4)]d_L$$
 (13)

$$-\frac{4}{t^2}\left[st\beta^2 + \frac{1}{2}(1+\beta^2)(ut - M_W^4)\right],\tag{14}$$

$$\frac{d\hat{\sigma}_{\text{TT}}}{dt} = \frac{\pi\alpha^2}{12s_W^4 \beta^4} \frac{ut - M_W^4}{s^4} \left[ \frac{1}{t^2} (u^2 + t^2 - 2M_W^4) \right]$$
 (15)

$$+\frac{\rho^4 s^2}{8} \left[ \frac{1}{(s-M_Z^2)^2} (d_L^2 + d_R^2) + 2 \frac{1}{s-M_Z^2} \frac{1}{t} d_L + \frac{1}{t^2} \right] \right], \tag{16}$$

where  $\rho = 2M_W/\sqrt{s}$  originating from the parameter b in Eq. (8),  $t = (q_1 - p_i)^2$  with  $p_i$  being the momentum of the W with the same sign of the electric charge as the quark,  $u = 2M_W^2 - s - t$  and

$$b_R = |e_q| \frac{s_W^2}{c_W^2} \beta^2 (3 - \beta^2), \quad b_L = b_R + \frac{1 - 2s_W^2}{c_W^2} + 2\rho^2, \tag{17}$$

$$d_R = 2|e_q| \frac{s_W^2}{c_W^2} \beta^2, \quad d_L = d_R + \frac{3 - 4s_W^2}{c_W^2}, \tag{18}$$

with  $s_W = \sin \theta_W$ ,  $c_W = \cos \theta_W$ ,  $\theta_W$  being the weak mixing angle,  $|e_q| = 2/3$  for up quarks, 1/3 for down quarks. Note that the L and R indices in these coupling parameters refer to the helicity of the incoming quarks. The total partonic cross section is obtained by integrating over  $t \in [-s(1+\beta)^2/4, -s(1-\beta)^2/4]$ . For the protonic cross section, a summation over the light quarks (with different weights proportional to the parton distribution functions (PDF)) and a further integration over  $s \in [4M_W^2, E_{CM}^2]$  are performed, where  $E_{CM} = \sqrt{s_{pp}}$  is the proton-proton colliding energy.

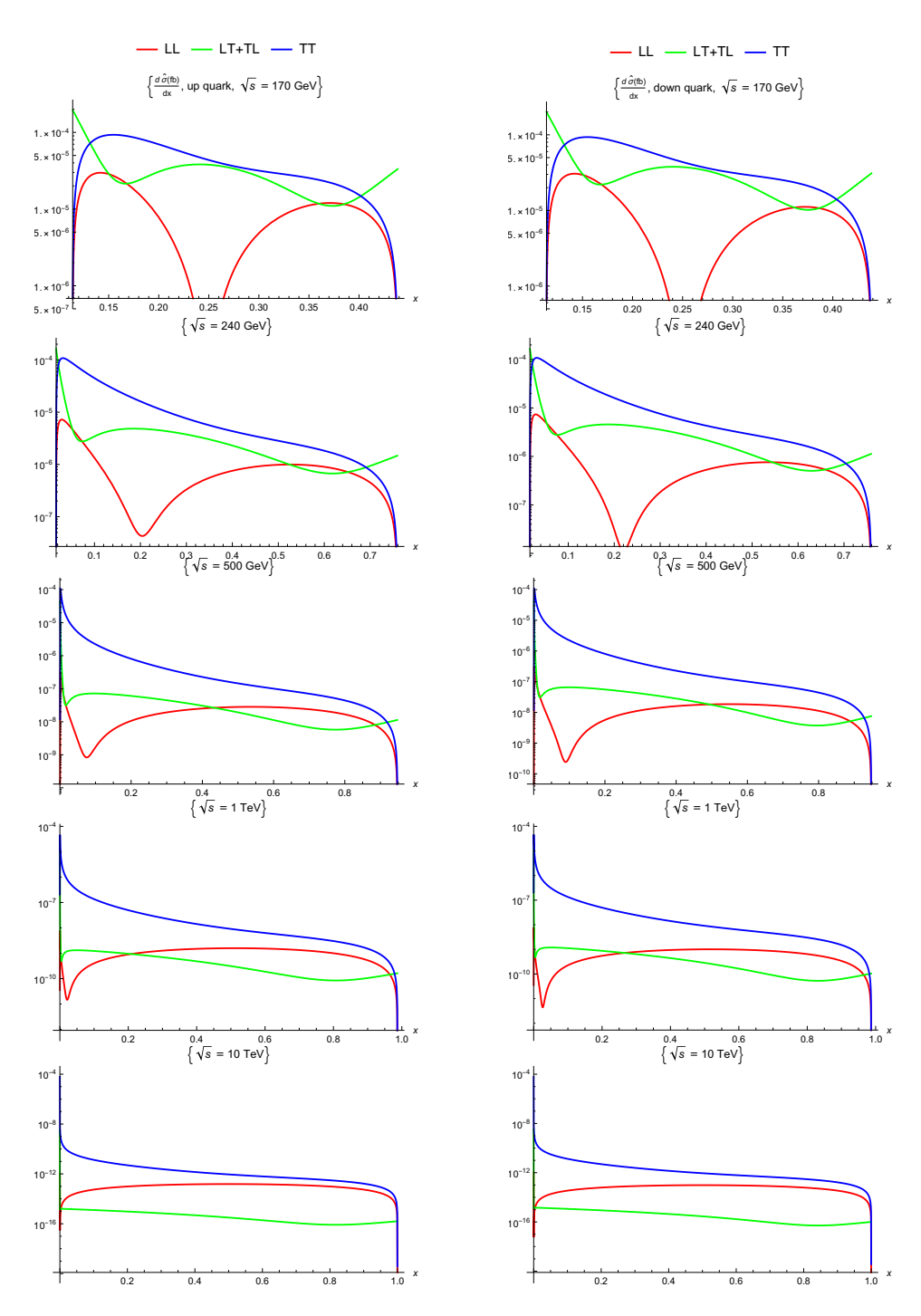


Fig. 2. (Color online) Polarized partonic cross sections as functions of the variable x = -t/s at increasing values of  $\sqrt{s}$ .

Note that the  $W_T^+W_L^-$  and  $W_L^+W_T^-$  cross sections are equal at the partonic level because of CP invariance, but become slightly different at the protonic level due to the PDFs.

We now consider the high energy limit of  $E \to \infty$ . The partonic cross sections in the region of  $|\cos \theta| \neq 1$  read:

$$\frac{d\hat{\sigma}_{LL}}{dt} \approx \frac{\pi\alpha^2}{48s_{W}^4} \frac{-st - t^2}{s^4} (a_L^2 + a_R^2),\tag{19}$$

$$\frac{d\hat{\sigma}_{\text{TL+LT}}}{dt} \approx \frac{\pi\alpha^2}{48s_W^4} \frac{4M_W^2}{s^3} \left[ (1 + \frac{2t}{s} + \frac{2t^2}{s^2})(c_L^2 + c_R^2) + \frac{4t}{s}c_L + 4 \right],\tag{20}$$

$$\frac{d\hat{\sigma}_{\text{TT}}}{dt} \approx \frac{\pi \alpha^2}{12s_W^4} \frac{-st - t^2}{s^4} (2 + \frac{2s}{t} + \frac{s^2}{t^2}),\tag{21}$$

with

$$a_R = 2|e_q|\frac{s_W^2}{c_W^2}, \quad a_L = a_R + \frac{1 - 2s_W^2}{c_W^2},$$
 (22)

$$c_R = 2|e_q|\frac{s_W^2}{c_W^2}, \quad c_L = c_R + \frac{3 - 4s_W^2}{c_W^2}.$$
 (23)

A few important remarks are in order. The 1/t pole does not occur in the LL and LT cases. This means that there is no enhancement in the region of small |t| where  $\cos \theta \approx 1$ . This enhancement is however very strong for the TT case. In the limit of  $E \to \infty$ , only the TL and LT cross sections vanish. Comparing the TT and LL cross sections, writing  $t \equiv -sx$ , we have

$$\frac{d\hat{\sigma}_{TT}}{d\hat{\sigma}_{LL}} \approx \frac{4}{a_t^2 + a_p^2} \left[ 1 + (1 - \frac{1}{x})^2 \right],\tag{24}$$

with  $x \in [\varepsilon, 1]$ ,  $\varepsilon > 0$  ( $\varepsilon = 0$  when  $s = \infty$  and  $\cos \theta = 1$ ). The prefactor  $4/(a_L^2 + a_R^2)$  is about 3.0 and 4.7, for up and down quarks respectively, explaining why the TT cross section is much larger than the LL one in the high energy region. We thus have the hierarchy of  $\hat{\sigma}_{TT} > \hat{\sigma}_{LL} > \hat{\sigma}_{LT+TL}$  in the high energy limit. The nonvanishing value of the LL cross section can be understood from the Goldstone equivalence theorem [38]. This theorem states that, in the high energy limit, the LL cross section is equal to the cross section of the  $q\bar{q} \to G^+G^-$  process (where  $G^\pm$  are the W Goldstone bosons), which does not vanish because of the s-channel  $\gamma/Z$ -exchange diagrams.

To understand the observed order of  $\sigma_{TT} > \sigma_{LT} > \sigma_{LL}$  as shown in Table 1 at the LHC we must consider the region of small s where the cross sections are largest. In Fig. 2, we show the partonic cross sections as functions of x for  $\sqrt{s} = 170\,\text{GeV}$ , 240 GeV, 500 GeV, 1 TeV, and 10 TeV, separately for two processes of  $u\bar{u}$  and  $d\bar{d}$ . We then integrate over x and show the  $M_{WW} = \sqrt{s}$  dependence in Fig. 3. Since the protonic cross section is a linear combination of the two plots in Fig. 3, with different weights depending on the value of  $\sqrt{s}$ , it has the same hierarchy of  $\hat{\sigma}_{TT}$ ,  $\hat{\sigma}_{LT}$  and  $\hat{\sigma}_{LL}$ . Taking into the PDFs, summing over the up and down quark contributions, and integrating over  $\sqrt{s}$  we then obtain the LO protonic cross sections, which have the hierarchy of  $\sigma_{TT} > \sigma_{LT} > \sigma_{LL}$  because the dominant contribution comes from the region of small  $\sqrt{s}$ . This also explains why the hierarchy does not change as the proton-proton colliding energy increases, as can be seen from Fig. 4 and Table 2.

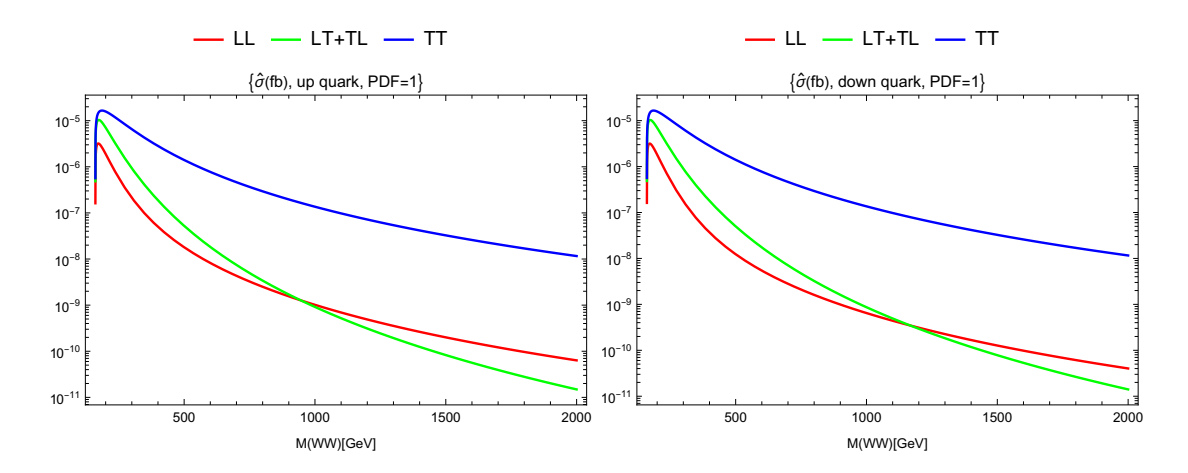
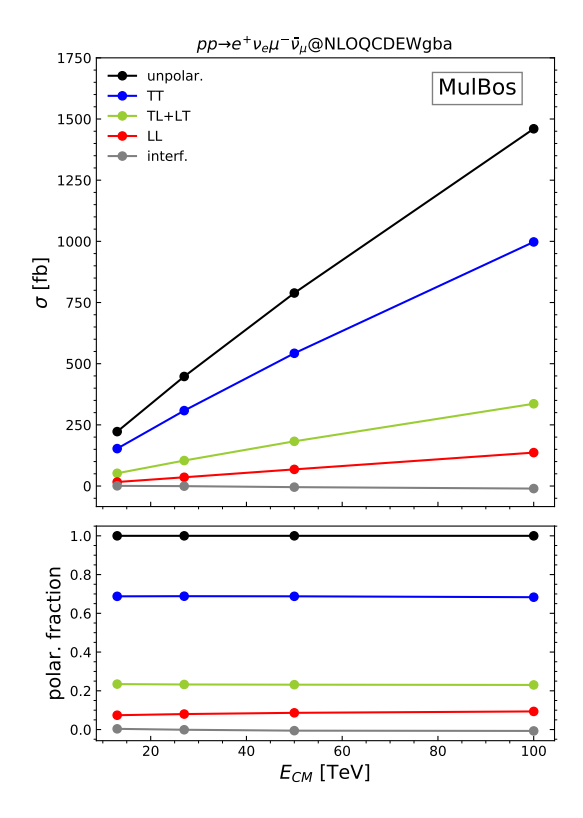


Fig. 3. (Color online) Polarized partonic cross sections as functions of the WW invariant mass.



**Fig. 4.** (Color online) Polarized cross sections as functions of the proton-proton center of mass energy. The corresponding polarization fractions are plotted in the small panel.

In Fig. 4 and Table 2 we show the dependence of the polarized cross sections and the corresponding polarization fractions on the proton-proton center of mass energy. The reference

Cross section [fb] Pol. fraction [%] 27 50 100 13 27 100  $E_{\rm CM}$  [TeV] 13 50 Unpolarized 222.41(3) 447.7(2) 788.8(4) 1460(1) 100 100 100 100 68.08(4)  $W_{I}^{+}W_{I}^{-}$ 16.46 35.80(2)136.62(8) 7.4 8.0 9.4 8.6 51.67(3) 90.93(5) 167.7(1)  $W_I^+W_T^-$ 25.75 11.6 11.5 11.5 11.5  $W_{T}^{+}W_{I}^{-}$ 26.43 52.50(3) 91.81(5) 168.6(1) 11.9 11.7 11.6 11.5  $W_{T}^{+}W_{T}^{-}$ 152.95(3) 308.2(2) 542.5(4) 997.6(8) 68.8 68.8 68.8 68.3 -0.10.81(4)-0.5(3)-4.5(6)-10(1)0.4 -0.6-0.7Interference

**Table 2.** Values of the polarized cross sections and the corresponding polarization fractions at 13, 27, 50, 100 TeV of the proton-proton center of mass energy.

energies of 27 TeV and 100 TeV are in accordance with the Future Circular Collider Conceptual Design Report [39]. Since the LT and TL lines almost coincide, they are combined in the plot for better visualization. Their individual values are given in Table 2. These results show that, except for the polarization interference, all the polarized cross sections scale up linearly with the colliding energy. As a consequence, the polarization fractions are flat. Most noticeable is the LL fraction, which goes very slightly upward, increasing from 7.4% at 13 TeV to 9.4% at 100 TeV. The polarization interference remains very small, being less than 1%, for the whole energy range.

We now discuss kinematic distributions. As an example, we show in Fig. 5 the differential distributions in the azimuthal-angle separation between the positron and the muon, for individual polarizations. In this distribution, we see two interesting features. First, the interference, which can be seen here as the difference between the unpolarized (black line) and the polarization sum (pink line) in the big panel, is quite large, in particular in the region of  $\Delta\phi\approx 2.5$  where it is about +12%. It changes sign at around  $\Delta\phi\approx 1.9$ , leading to a very small effect in the integrated cross section. Second, the  $\bar{\delta}_{b\bar{b}}$  correction for the LL case increases with the separation, reaching +20% at  $\Delta\phi\approx 2.5$ . Remarkably, this behavior does not change when NLO corrections are included for the bottom-induced processes, as can be seen in Fig. 7 of [14].

Finally, we show in Table 3 the comparison between our results (denoted by superscript DL) and Ref. [12] (denoted DHP) using the input setup of [12], at LO and NLO EW.

While the LO agreements are very good, being within 2 standard deviations and with differences smaller than 1 per-mille; the NLO EW comparisons are not as good. The largest discrepancy

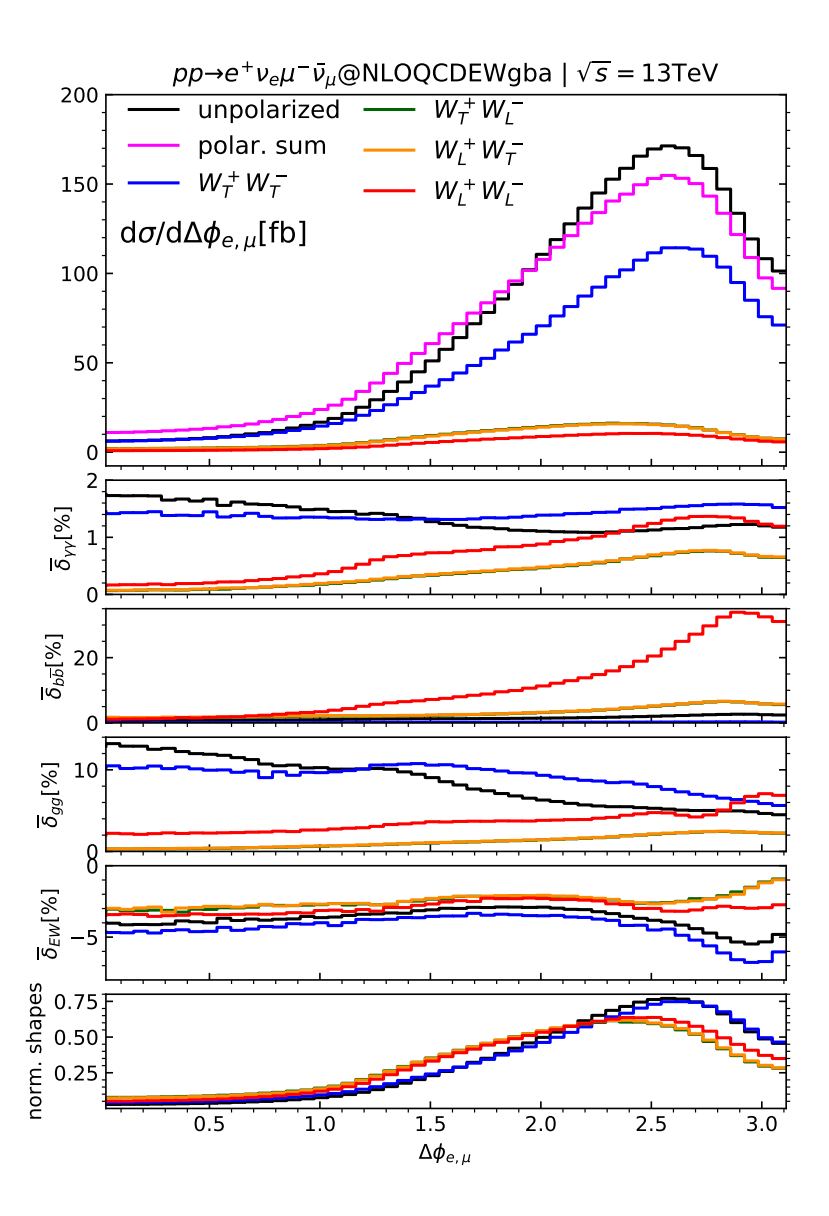


**Fig. 5.** (Color online) Distributions in the azimuthal-angle separation  $\Delta\phi_{e,\mu}$ . The big panel shows the absolute values of the cross sections including all contributions from the  $q\bar{q}$ , gg,  $b\bar{b}$ ,  $\gamma\gamma$  processes. The middle panels display the corrections with respect to the NLO QCD  $q\bar{q}$  cross sections. The bottom panel shows the normalized shapes of the distributions plotted in the top panel. Taken from [13].

is found for the TT polarization at the level of -0.4%. In terms of standard deviation, it is  $27\sigma$ . Compared to the scale uncertainties shown in Table 1, this tiny difference is numerically irrelevant. Conceptually, this difference may indicate different implementations of the DPA by the

two groups. More thorough investigations are currently underway to resolve these discrepancies between the two results.

**Table 3.** Comparison between Ref. [13] (indicated by the superscript DL) and Ref. [12] (indicated by the superscript DHP) for the  $W^+W^-$  process in the WW CM frame at LO and NLO EW levels. The difference is defined as  $\Delta = (\sigma^{DL} - \sigma^{DHP})/\sigma^{DHP}$ . Note: the  $\gamma\gamma$  channel is calculated at LO;  $b\bar{b}$ ,  $b\gamma$ , gg are excluded. The DHP results are obtained from Table 1 of Ref. [12] and the  $\gamma\gamma$  cross sections (LO and NLO EW) from private communication.

	$\sigma_{ m LO}^{ m DL}[{ m fb}]$	$\sigma_{ m LO}^{ m DHP}[{ m fb}]$	$\Delta_{ ext{LO}}[\%]$	$\sigma_{ m NLO}^{ m DL}[ m fb]$	$\sigma_{ m NLO}^{ m DHP}[{ m fb}]$	$\Delta_{ m NLO}[\%]$
unpolar. (DPA)	245.6(1)	245.79(2)	-0.07	240.56(3)	241.32(2)	-0.3
LL	18.75(1)	18.752(2)	-0.006	18.497(2)	18.499	-0.01
LT	32.07(2)	32.084(3)	-0.04	31.998(4)	32.032	-0.1
TL	33.21(2)	33.244(5)	-0.09	33.106(4)	33.144	-0.1
TT	182.0(1)	182.17(2)	-0.07	176.93(2)	177.70(2)	-0.4

### 4. Conclusions

In this contribution, we have presented the NLO QCD+EW results for polarized  $W^+W^-$  pairs produced at the LHC with a fully leptonic final state. A comparison between our results and the ones of Ref. [12] has been performed, showing good agreements. These results complete the polarized calculation of all diboson processes ZZ, WZ, and  $W^+W^-$ , being now achieved at the NLO QCD+EW level. The next step is to implement these calculations into event generators where parton shower and hadronization are incorporated, so that experimental colleagues can perform simulations for their measurements.

## Acknowledgements

We would like to thank the organizers of this conference for organizing this wonderful event and the nice atmosphere. We are grateful to Ansgar Denner and Giovanni Pelliccioli for helpful discussions and providing us results for the comparison with Ref. [12]. This research is funded by Phenikaa University under grant number PU2023-1-A-18.

#### Conflict of interest

The authors have no conflict of interest to declare.

#### References

- [1] OPAL Collaboration, Measurement of W boson polarizations and CP violating triple gauge couplings from W<sup>+</sup>W<sup>-</sup> production at LEP, Eur. Phys. J. C 19 (2001) 229.
- [2] DELPHI Collaboration, Correlations between polarisation states of W particles in the reaction  $e^-e^+ \rightarrow w^-w^+$  at LEP2 energies 189 GeV 209 GeV, Eur. Phys. J. C **63** (2009) 611.
- [3] ATLAS Collaboration, Observation of gauge boson joint-polarisation states in W<sup>±</sup>Z production from pp collisions at  $\sqrt{s} = 13$  TeV with the ATLAS detector, Phys. Lett. B **843** (2023) 137895.

- [4] ATLAS Collaboration, Studies of the energy dependence of diboson polarization fractions and the radiation amplitude zero effect in WZ production with the ATLAS detector, JHEP (2024) 169901.
- [5] ATLAS Collaboration, Evidence of pair production of longitudinally polarised vector bosons and study of CP properties in  $ZZ \rightarrow 4\ell$  events with the ATLAS detector at  $\sqrt{s} = 13$  TeV, JHEP (2023) 107.
- [6] CMS Collaboration, Measurements of production cross sections of polarized same-sign W boson pairs in association with two jets in proton-proton collisions at  $\sqrt{s} = 13$  TeV, Phys. Lett. B **812** (2021) 136018.
- [7] A. Denner and G. Pelliccioli, NLO EW and QCD corrections to polarized ZZ production in the four-charged-lepton channel at the LHC, JHEP 10 (2021) 097.
- [8] A. Denner and G. Pelliccioli, NLO QCD predictions for doubly-polarized WZ production at the LHC, Phys. Lett. B 814 (2021) 136107.
- [9] D. N. Le and J. Baglio, Doubly-polarized WZ hadronic cross sections at NLO QCD + EW accuracy, Eur. Phys. J. C 82 (2022) 917.
- [10] D. N. Le, J. Baglio and T. N. Dao, Doubly-polarized WZ hadronic production at NLO QCD+EW: calculation method and further results, Eur. Phys. J. C 82 (2022) 1103.
- [11] A. Denner and G. Pelliccioli, *Polarized electroweak bosons in w+ w- production at the lhc including nlo qcd effects*, Journal of High Energy Physics **2020** (2020) 1.
- [12] A. Denner, C. Haitz and G. Pelliccioli, *NLO EW corrections to polarised W*<sup>+</sup>*W*<sup>-</sup> *production and decay at the LHC*, Phys. Lett. B **850** (2024) 138539.
- [13] T. Dao and D. Le, *NLO electroweak corrections to doubly-polarized W*<sup>+</sup>*W*<sup>-</sup> *production at the LHC*, Eur. Phys. J. C **84** (2024) 244.
- [14] T. Dao and D. Le, Polarized  $W^+W^-$  pairs at the LHC: Effects from bottom-quark induced processes at NLO QCD+EW, Phys. Lett. B 85 (2025) 108.
- [15] R. Poncelet and A. Popescu, NNLO QCD study of polarised W<sup>+</sup>W<sup>-</sup> production at the LHC, JHEP **07** (2021) 023.
- [16] A. Denner, C. Haitz and G. Pelliccioli, NLO QCD corrections to polarized diboson production in semileptonic final states, Phys. Rev. D 107 (2023) 053004.
- [17] A. Denner, D. Lombardi, S. Chavez and G. Pelliccioli, *NLO corrections to triple vector-boson production in final states with three charged leptons and two jets*, JHEP **2024** (2024) 187.
- [18] A. Denner, D. Lombardi and C. Schwan, *Double-pole approximation for leading-order semi-leptonic vector-boson scattering at the LHC*, JHEP **08** (2024) 146.
- [19] M. Hoppe, M. Schönherr and F. Siegert, Polarised cross sections for vector boson production with SHERPA, Phys. Lett. B 2024 (2024) 1.
- [20] G. Pelliccioli and G. Zanderighi, Polarised-boson pairs at the LHC with NLOPS accuracy, Phys. Lett. B 84 (2024) 16.
- [21] M. Javurkova, R. Ruiz, R. de Sá and J. Sandesara, *Polarized ZZ pairs in gluon fusion and vector boson fusion at the LHC*, Phys. Lett. B **855** (2024) 138787.
- [22] A. Aeppli, F. Cuypers and G. van Oldenborgh,  $\mathcal{O}(\gamma)$  corrections to w pair production in  $e^+e^-$  and  $\gamma\gamma$  collisions, .
- [23] A. Aeppli, G. van Oldenborgh and D. Wyler, Unstable particles in one loop calculations, Nucl. Phys. B 428 (1994) 126.
- [24] A. Denner, S. Dittmaier, M. Roth and D. Wackeroth, *Electroweak radiative corrections to*  $e^+e^- \rightarrow WW \rightarrow 4$  fermions in double pole approximation: The RACOONWW approach, Nucl. Phys. B **587** (2000) 67.
- [25] S. Catani and M. Seymour, A General algorithm for calculating jet cross-sections in NLO QCD, Nucl. Phys. B 485 (1997) 291.
- [26] S. Catani, S. Dittmaier, M. Seymour and Z. Trocsanyi, The Dipole formalism for next-to-leading order QCD calculations with massive partons, Nucl. Phys. B 627 (2002) 189.
- [27] S. Dittmaier, A General approach to photon radiation off fermions, Nucl. Phys. B 565 (2000) 69.
- [28] L. Basso, S. Dittmaier, A. Huss and L. Oggero, Techniques for the treatment of IR divergences in decay processes at NLO and application to the top-quark decay, Eur. Phys. J. C 76 (2016) 56.
- [29] A. Denner, Techniques for calculation of electroweak radiative corrections at the one loop level and results for W physics at LEP-200, Fortsch. Phys. 41 (1993) 307.
- [30] T. Hahn, Generating Feynman diagrams and amplitudes with FeynArts 3, Comput. Phys. Commun. 140 (2001) 418.

- [31] T. Hahn and M. Perez-Victoria, Automatized one-loop calculations in four and D dimensions, Comput. Phys. Commun. 118 (1999) 153.
- [32] G. Passarino and M. Veltman, One Loop Corrections for  $e^+e^-$  Annihilation Into  $\mu^+\mu^-$  in the Weinberg Model, Nucl. Phys. B **160** (1979) 151.
- [33] G. 't Hooft and M. Veltman, Scalar one loop integrals, Nucl. Phys. B 153 (1979) 365.
- [34] D. Nhung and L. Ninh, DOC: A code to calculate scalar one-loop four-point integrals with complex masses, Comput. Phys. Commun. 180 (2009) 2258.
- [35] A. Denner and S. Dittmaier, Scalar one-loop 4-point integrals, Nucl. Phys. B 844 (2011) 199.
- [36] S. Kawabata, A New version of the multidimensional integration and event generation package BASES/SPRING, Comput. Phys. Commun. 88 (1995) 309.
- [37] J. Baglio, F. Campanario, T. Chen, H. Dietrich-Siebert, T. Figy, M. Kerner *et al.*, *Release note: Vbfnlo 3.0*, The European Physical Journal C **84** (2024) 1003.
- [38] S. Willenbrock, Pair Production of W and Z Bosons and the Goldstone Boson Equivalence Theorem, Annals Phys. **186** (1988) 15.
- [39] FCC Collaboration, *HE-LHC: the high-energy large hadron collider: future circular collider conceptual design report volume 4*, Eur. Phys. J. ST **228** (2019) 1109.